JOURNAL OF GEOPHYSICAL RESEARCH, VOL. 102, NO. B6, PAGES 11,815–11,827, JUNE 10, 1997

Variations of *P* wave speeds in the mantle transition zone beneath the northern Philippine Sea

Michael R. Brudzinski and Wang-Ping Chen[1]
Department of Geology, University of Illinois, Urbana

Robert L. Nowack
Department of Earth and Atmospheric Sciences, Purdue University, West Lafayette, Indiana

Bor-Shouh Huang
Institute of Earth Sciences, Academia Sinica, Taipei, Taiwan

Abstract. Using waveforms and travel times from deep earthquakes, we constructed 16 seismic profiles, each of which constrains the radial variation in V_p over a small area beneath the northern Philippine Sea. Taken together, the azimuthal coverage of these profiles also places tight bounds on the lateral extent of a region of anomalously high V_p (up to 3% faster than average Earth models) originally suggested by travel time tomography. Unlike travel time tomography, which relies heavily on arrival times of the direct *P* phase, we utilize the waveforms and move-out of later arrivals that mainly sample the mantle transition zone of interest. Our results identify three important characteristics of the northern Philippine Sea anomaly that are distinct from previous results. First, being approximately a subhorizontal, laterally uniform feature, the anomaly is localized beneath the northwestern corner of the Philippine Sea, within a region of approximately 500 × 500 km^2 immediately east of the Ryukyu arc. Second, the anomaly is well constrained to occur in the lower portion of the transition zone, extending all the way down to the 660-km discontinuity. Third, the presence of such a distinct anomaly reduces the contrast in V_p across the 660-km discontinuity from approximately 6% to 3%. Such a configuration is consistent with the interpretation that the anomaly is caused by a remnant of subducted slab, as negative buoyancy should rest the slab just above the 660-km discontinuity where resistance to subduction is expected from a negative Clapeyron slope during the spinel–Mg-Fe-perovskite transition.

Introduction

The fate of subducted lithosphere is one of the fundamental issues in geophysics and geochemistry. In particular, the depth of penetration of subducted lithosphere constrains the extent of heat and mass transfer between the upper and the lower mantle [e.g., *Anderson*, 1989; *Lay*, 1994; *Silver et al.*, 1988]. Several recent studies showed evidence that the extent of slab penetration into the lower mantle seems to vary laterally along subduction zones such that at least some subducted slabs remain stagnant in the upper mantle [e.g., *Glennon and Chen*, 1995a; *Ding and Grand*, 1994], while others plunge steeply into the lower mantle [e.g., *Jordan*, 1977; *Creager and Jordan*, 1984, 1986]. For instance, on the basis of long-period (~20 s) converted and reflected body waves, *Shearer and Masters* [1992] and *Shearer* [1991] contended that the topography of the 660-km discontinuity shows large-scale depressions extending over a width of approximately 2000 km across the Kuril and northern Japan subduction zones. Such a feature is expected if cold, subducted lithosphere of the Pacific is trapped just above the 660-km discontinuity.

Recent images from travel time tomography beneath the western Pacific also suggested that large, subhorizontal regions of anomalously fast *P* wave speed (V_p), interpreted as subducted material, exist in the transition zone of the mantle (i.e., the zone between depths of approximately 400 and 660 km) [*Fukao et al.*, 1992; *van der Hilst et al.*, 1991, 1993]. The anomaly is most pronounced under the northern portion of the Philippine Sea plate, with a V_p of up to 3% faster than average Earth models. In map view this feature seems to extend westward for almost 2000 km, from the tip of the Izu–Bonin Wadati-Benioff zone to the back arc region of the Ryukyu–Kyushu trench where the Philippine Sea plate subducts beneath Eurasia. If this is true, both the magnitude of lateral variations in V_p and the spatial extent of the anomaly beneath the northern Philippine Sea region are among the most pronounced in the transition zone of the mantle.

In detail the geometry of this anomaly suggested by tomography is peculiar. Instead of resting just above the

[1] Also at Department of Theoretical and Applied Mechanics, University of Illinois, Urbana.

Paper number 97JB00212.
0148-0227/97/97JB-00212$09.00

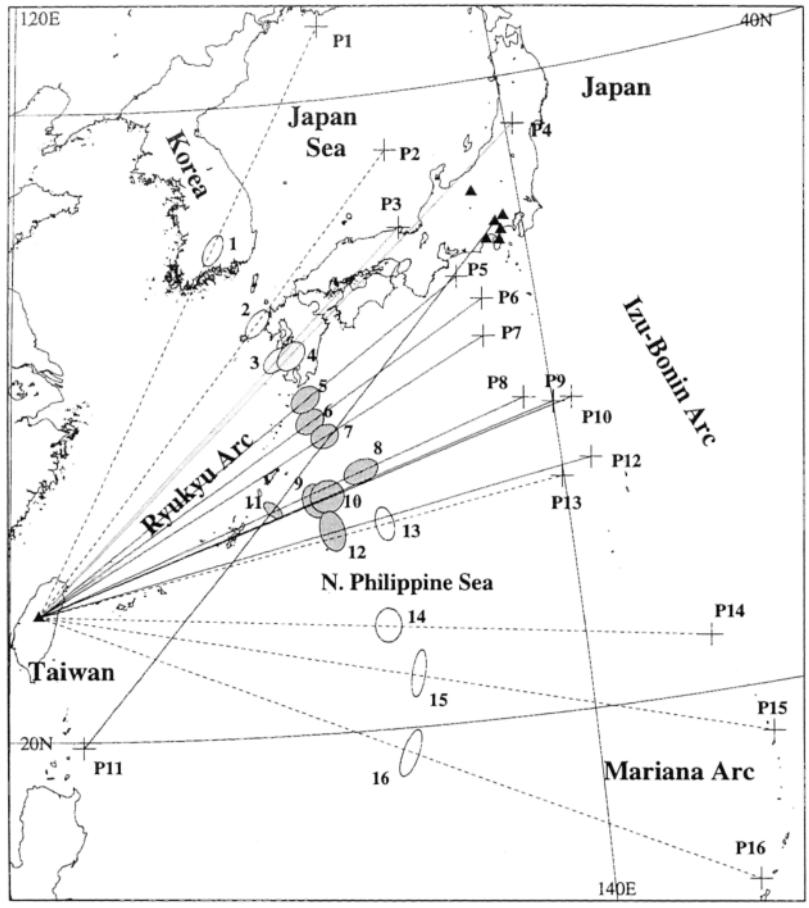

Figure 1. Map showing the configuration and main results of the northern Philippine Sea experiment. Triangles mark the center of the CWB-TTSN short-period array and the locations of broadband stations of the Pre-POSEIDON array used in this study. Crosses mark epicenters of 16 intermediate- and deep-focus earthquakes (Table 1) used to construct the seismic profiles (P1–P16). Ellipses show approximate locations of the mantle transition zone sampled by turning rays along the 16 seismic profiles. Each ellipse is numbered according to its associated profile. For regions 5–12 (dark shading), V_p in the lower portion of the mantle transition zone is approximately 2% faster than the iasp91 average Earth model, while V_p in regions 1–2 and 13–16 (no shading) are close to the iasp91 model. V_p in regions 3 and 4 (light shading) appear to fall somewhere in between the two extremes. The azimuthal equidistant projection is centered at the symbol for the CWB-TTSN array.

660-km discontinuity, the most pronounced anomalies are reported to occur between depths of 490–570 km, in the middle of the transition zone [*van der Hilst et al.*, 1993]. If the anomalies are indeed caused by subducted Pacific lithosphere, the tomographic images seem to imply that a remnant of the slab either encountered strong resistance to subduction in the middle of the transition zone or may even have become positively buoyant in a time period of the order of only 10 million years after subduction. Either scenario seems unusual.

To investigate the nature of this anomaly in V_p, we utilized waveform and travel time data from two seismic arrays near the edges of the Philippine Sea: the Pre-POSEIDON broadband seismic network of Japan and the short-period Central Weather Bureau and Taiwan Telemetered Seismograph Network (CWB-TTSN) (Figure 1). The Philippine Sea plate is surrounded by several Wadati-Benioff zones of high background seismicity. For many earthquakes at epicentral distances of approximately 15°–25° from the arrays (Figure 2), turning points of rays that comprise the *P* wave train primarily sample the mantle transition zone where the most pronounced lateral and radial variations in V_p have been suggested by tomography.

Unlike in travel time tomography, which relies heavily on arrival times of the direct *P* phase reported in bulletins, we emphasize the rich information contained in the waveform and move-out (i.e., changes in arrival times with respect to distance) of later arrivals that mainly sample the depths of interest. This work complements the previous studies by providing resolution on several aspects of the anomaly that are of particular interest to geodynamics. For instance, our results indicate that the anomaly of fast V_p seems to occur in the lower portion of the transition zone, reducing the contrast in V_p across the 660-km discontinuity to approximately 3%. The lateral extent of the anomaly is constrained to be mainly beneath the northwestern corner of the Philippine Sea, immediately to the east of the Ryukyu–Kyushu trench. Moreover, if the fast V_p is associated with subducted Pacific lithosphere, cold

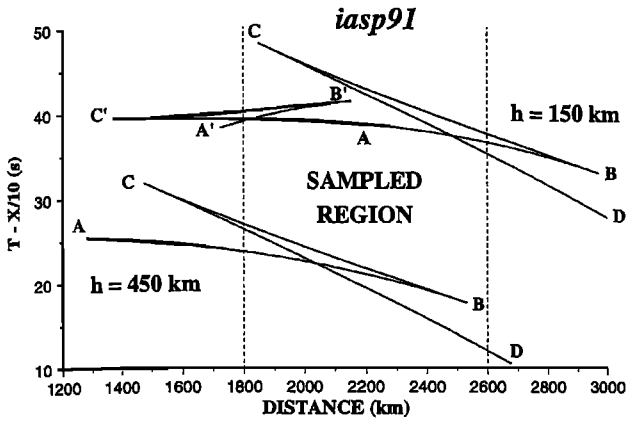

Figure 2. Triplication of travel time curves due to discontinuities near the transition zone of the mantle, as predicted by the iasp91 model. Travel time curves for two representative focal depths (h) are plotted. Events that occur below the 400-km discontinuity will exhibit only one triplication caused by the 660-km discontinuity. Branches within this triplication are labeled according to standard nomenclature: branch AB, continuous refraction turning above the discontinuity; branch BC, pseudo-reflections off the discontinuity; and branch CD, continuous refraction turning below the discontinuity. Triplicated branches from the 400-km discontinuity are labeled by primed letters. All figures displaying travel time curves (2–3, 5–11) are plotted with a reduction speed of 10 km/s.

temperature in the slab may not be sufficient to fully account for the large magnitude of the anomaly, suggesting the presence of depleted mantle material.

Data and Analysis

To constrain three-dimensional variations of V_p in the mantle transition zone beneath the northern Philippine Sea, we constructed 16 seismic profiles over a range of azimuths (Figure 1). While each individual profile mainly constrains the radial variation in V_p over a small area, the azimuthal coverage of the profiles places bounds on the lateral extent of anomalies in V_p.

We used digital signals that originated from deep- and intermediate-depth earthquakes around the northern Philippine Sea (Table 1). These signals were recorded by two separate, regional seismic arrays. The Pre-POSEIDON array of Japan consists of approximately 12 broadband (high-resolution) seismographs near the northern edge of the target region (Figure 1). The broad bandwidth and high dynamic range of these stations are highly effective in recording seismic signals from all distance ranges. For this reason, we were able to use travel time residuals from distant earthquakes to remove near-station structural effects (station corrections). For a given observed seismic profile we found that one-dimensional models of radially varying V_p are sufficient to explain the observed waveforms. These waveforms include all relevant arrivals from triplications of the travel time curves that are caused by discontinuities in the transition zone of the mantle (Figure 2). For this data set, slowness of the P wave at particular depths in the transition zone is directly determined by the move-out of first arrivals over the array.

Since data from most stations of the Pre-POSEIDON array were not available until May 1993, we also used a large number of short-period, digital seismograms recorded in Taiwan by the CWB-TTSN, available since 1987. This is a dense array of approximately 75 stations distributed in and around Taiwan near the western edge of our target region (Figure 1). The primary purpose of this array is to record regional and local earthquakes. Data from few teleseismic events are retained. Consequently, we cannot obtain station corrections to account for structural heterogeneity within the CWB-TTSN array. Instead we utilized the relative timing and move-out of later arrivals with respect to those of the first arrivals.

Table 1. Summary of Source-Receiver Geometry

Event Information						Profile Information				
Date	Origin Time[a], UT	Latitude[a], °N	Longitude[a], °E	Depth[a], km	m_b[a]	Profile	Back Azimuth, deg	Epicentral Distances, km	Sampled Depths[b], km	Preferred Model
July 21, 1994	1836:32	42.34	132.87	471	6.5	P1	25	2210–2520	593–728	iasp
Mar. 31, 1995	1401:40	38.21	135.01	354	6.0	P2	37	1910–2256	477–683	iasp
Aug. 7, 1992	1111:42	35.73	135.15	358	5.6	P3	43	1750–2060	458–670	•••
Jan. 22, 1992	0106:56	38.47	140.31	116	5.6	P4	44	2301–2610	380–679	•••
July 7, 1995	2115:19	33.97	137.13	333	5.8	P5	51	1767–2097	442–670	C34
Aug. 29, 1992	1919:06	33.19	137.98	289	6.0	P6	55	1797–2097	366–664	C34
Oct. 11, 1993	1554:21	32.02	137.83	351	6.4	P7	58	1730–2024	474–664	C34
Oct. 30, 1992	0249:48	29.94	138.98	393	6.0	P8	66	1730–2120	495–670	C34
Dec. 12, 1987	0451:51	29.69	140.02	164	6.3	P9	67	1854–2103	304–660	C34
June 1, 1992	1829:20	29.74	140.70	134	5.5	P10	68	1919–2207	304–662	C34
May 18, 1993	1019:34	19.91	122.45	169	6.4	P11	40[c]	2298–2401	400–671	C34
Dec. 3, 1988	0313:46	27.80	141.06	106	5.5	P12	74	1948–2168	298–660	C34
Oct. 2, 1987	0738:28	27.35	139.94	463	5.5	P13	75	1810–2050	516–680	iasp
July 22, 1993	1215:36	21.76	144.26	127	5.6	P14	91	2300–2541	480–685	iasp
May 4, 1988	2347:02	18.51	145.86	122	5.9	P15	99	2564–2684	545–700	iasp
Feb. 10, 1991	1415:20	14.01	144.74	156	5.5	P16	110	2609–2750	558–708	iasp

[a] Values of parameters are from the monthly listing of *Preliminary Determination of Epicenters* (PDE).

[b] Range of bottoming depths for the rays comprising the P wave train, including all branches of traveltime triplication sampled by each profile.

[c] Azimuth, not back azimuth, is the appropriate parameter used for this profile.

To combine data from these two arrays, our analysis proceeded as follows. First, we searched for broadband seismograms from the Pre-POSEIDON project, concentrating on data from intermediate- and deep-focus earthquakes that occurred approximately 20°±5° away from the densely spaced stations in central Japan (Figure 1). In this epicentral distance range, turning points of rays that comprise the P wave train occur in the transition zone of the mantle (Figure 2). We selected the azimuthal range of profiles such that these turning points fall near the region in which the most pronounced anomaly of fast V_p beneath the northern Philippine Sea has been suggested by travel time tomography (Figure 1). By using only data from earthquakes deeper than 100 km we minimized any potential effects of structural complexity above the source. For each profile, observed waveforms were then matched by synthetic seismograms to generate a working model of V_p. We found that simple, laterally homogeneous models are sufficient to explain each observed profile, and there is no evidence to suggest that more complex models are necessary. Obviously, each of the laterally homogeneous models is appropriate only in the vicinity of the region sampled by a particular profile.

Next we turn to profiles constructed from the CWB-TTSN short-period data that sample approximately the same portion of the mantle as do broadband waveforms obtained from the Pre-POSEIDON seismic array. Along a given profile using CWB-TTSN data, the first arrival time at each station is manually picked and then time corrected to that predicted by the working model on the basis of broadband (Pre-POSEIDON) data. Observed arrival times of later arrivals and move-out with respect to the first arrivals are then compared with those predicted by the working model. Whenever possible, observed short-period waveforms are also compared with synthetic seismograms generated from this working model. Each working model originally developed from Pre-POSEIDON data is modified iteratively until synthetic seismograms and predicted arrival times generated from the model match both the broadband and short-period profiles. This entire process is repeated for different geographic regions sampled by distinct profiles. Additional details on the processing of broadband and short-period data are presented in Appendices A and B, respectively.

Results

In the region sampled by our data where V_p is anomalously high, one-dimensional models are sufficient to explain each seismic profile. Furthermore, a single, uniform model can adequately represent the entire anomalous region as a laterally homogeneous structure, referred to as the northern Philippine Sea anomaly. Within this anomaly our data placed constraints on the slowness of the P wave, the vertical gradient of V_p in the transition zone, and the change in V_p across the 660-km discontinuity. The lateral extent of the anomaly is constrained by surrounding profiles that can be explained well by average Earth models (Figure 1). Since it is not the purpose of this study to investigate average Earth models, in the following discussions we have used the iasp91 model [*Kennett and Engdahl*, 1991] that happens to be suitable for profiles surrounding the northern Philippine Sea anomaly.

Northern Philippine Sea Anomaly

Broadband Data. In the short time period since Pre-POSEIDON data became available, profile 11 is the only broadband data set we identified that directly sampled the northern Philippine Sea anomaly (Figure 1). Twelve stations in the Pre-POSEIDON array recorded the event. Among them, excellent data with high signal-to-noise ratios (S/N) are available from six stations near Tokyo, with an average spacing of only 20 km over an aperture of 100 km (Figure 3). The source-receiver geometry is approximately linear, within 10° in back azimuthal range from the source (Figure 1).

Data shown in Figure 3 have been corrected for static time shifts due to near-station structure. Waveforms have been deconvolved to remove effects of a finite earthquake source whose parameters, in turn, were precisely determined by the inversion of teleseismic waveforms following a procedure described by *Glennon and Chen* [1993, 1995b]. During deconvolution the data are band-pass filtered between 0.75 and 0.1 Hz. The layout of the final data set places an arrival from a forward branch of a

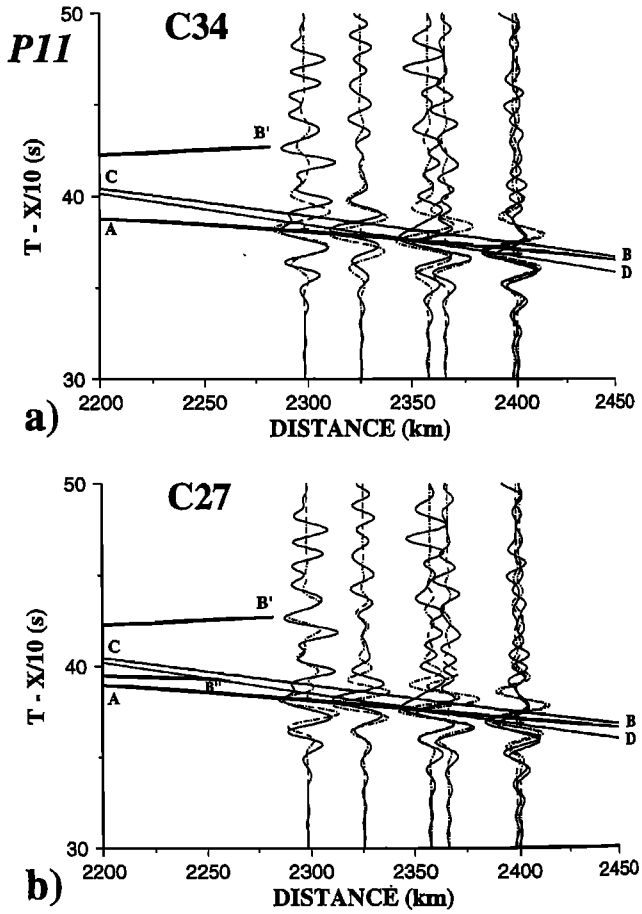

Figure 3. Comparisons between observed (solid traces) and synthetic (dash-dotted traces), broadband seismograms from the Pre-POSEIDON array along profile 11. Smooth curves show predicted travel times, while solid dots show visually picked first arrivals from unprocessed seismograms. (a) The simple model C34 (Figure 4). (b) Model C27 with a 520-km discontinuity (Figure 4). At the near end of the array the cusp (B") produced by the 520-km discontinuity provides a good fit to the beginning of the waveform.

triplication as a peak of an acausal, symmetric wavelet. For comparison, visually picked first arrivals are also plotted (Figure 3). The deconvolved data set is used for waveform analysis. Details of data processing are presented in Appendix A.

Given the approximate linear geometry of each profile in Figure 1, we calculated synthetic seismograms using the WKBJ algorithm [*Chapman*, 1978; *Chapman et al.*, 1988]. We performed both forward modeling and waveform inversion to find the best fitting models, and the results from both approaches are similar. Each model of V_p is subject to a priori constraints regarding its gradient with respect to depth in the transition zone, contrasts in V_p across major discontinuities, and depths of such discontinuities. We used bounds on these parameters summarized by *Kennett* [1993]. The best fitting model is then perturbed by forward modeling to estimate uncertainties of parameters.

In Figure 3, move-out of first arrivals across the Pre-POSEIDON array is approximately 10 km/s (in a spherical Earth). This apparent speed and the distance range over which the speed is measured indicate that these arrivals mainly sample the middle to lower portion of the transition zone. Indeed, results of modeling the waveforms show that the largest arrivals are from refractions turning in the middle of the transition zone (branch AB, Figure 3a). The precise depths for the turning points of rays are model dependent. We found the V_p to be 10.0±0.13 km/s at a depth of approximately 580±15 km.

With a Nyquist frequency of 10 Hz in the raw data the high S/N of the data can resolve differences as small as 0.2–0.3 s in travel times between observed and synthetic waveforms. Thus, observed first arrivals are sensitive to changes in the gradient of V_p with respect to depth. Given the limited aperture of the Pre-POSEIDON array, however, a more robust constraint on the gradient comes from the near end of the array, where a conspicuous secondary arrival is identified to be the caustic arrival from the 400-km discontinuity (cusp B', Figures 2 and 3).

In addition to the fact that synthetic seismograms match observed waveforms from this cusp (Figure 3b), the identification of the location of cusp B' is corroborated by short-period seismograms from Taiwan along profiles 10 and 5 to be discussed in Figures 5 and 11, respectively. Timing of this cusp gives an estimate of the root-mean-square (RMS) V_p above the 400-km discontinuity. Taken together with the timing and move-out of the first arrivals, the observed waveforms can only be matched with a steep gradient in V_p across the transition zone. This feature is illustrated when one compares the iasp91 model, a commonly used one-dimensional, radially varying model representing the average V_p of the Earth, with our preferred model, C34, which is used to generate synthetic seismograms in Figure 3a (Figure 4).

Notice that the identification of cusp B' in the data constrains only the RMS V_p above the 400-km discontinuity. Thus in model C34, variations in V_p above depths of 400 km are simply taken from the model of *Erdogan and Nowack* [1993], the most recent, average model for the Philippine Sea area as a whole. Similarly, since there is no indication from travel time tomography that any anomaly in V_p exists in the lower mantle beneath the entire Philippine Sea [*Fukao et al.*, 1992; *van der Hilst et al.*, 1991, 1993], we assumed that V_p in the lower mantle is adequately represented by the iasp91 model. As a result we have varied only values of V_p and the thickness of the transition zone in our modeling. In the simplest case of a single layer in the transition zone such as model C34, there are only four free parameters: depths to and contrasts in V_p across the 400- and 660-km discontinuities, all subject to a priori constraints discussed earlier in this section.

Under these conditions a steep linear gradient of approximately $5.35\pm0.3 \times 10^{-3}$ km/s/km appears to be required to explain the data, and model C34 is our best fitting model. Overall features of observed waveforms are matched by synthetic seismograms generated from this model, with a maximum mismatch in timing of only 0.2 s (Figure 3a). The only noticeable mismatch in the waveforms is at the near end of the array at a distance of 2300 km. For this station a prominent peak arrives approximately 1 s after the first arrival. Since no such arrival is expected if the entire transition zone is represented by a single layer, the most straightforward interpretation of this mismatch is to introduce a small discontinuity in the middle of the transition zone. This procedure results in two additional free parameters, the contrast in V_p and the depth to the discontinuity.

Following the work of *Shearer* [1990, 1991] and *Revenaugh and Jordan* [1991], we experimented with

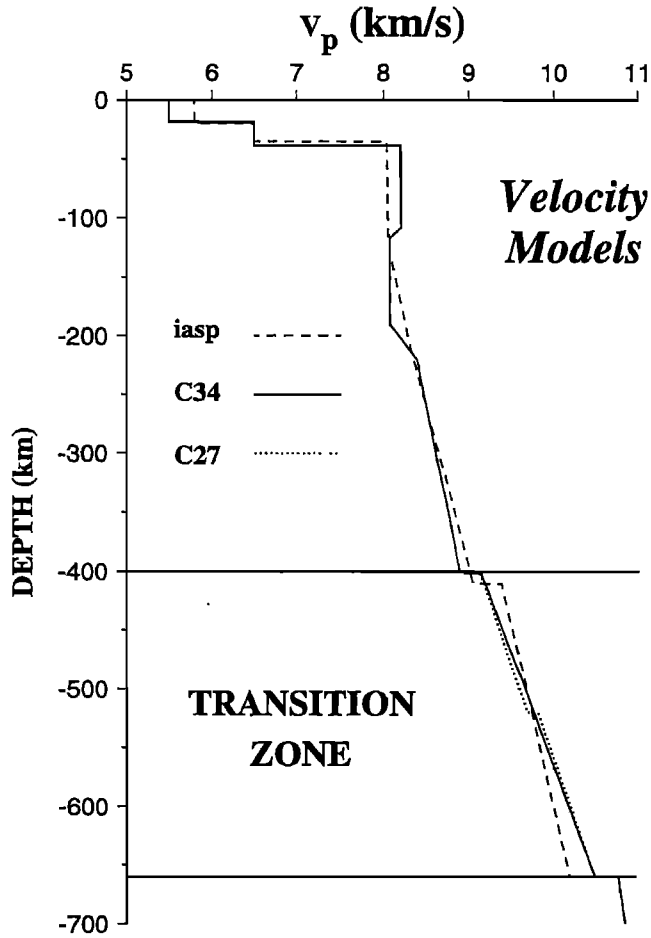

Figure 4. Comparison of three models for V_p in the upper mantle. Both models C34 and C27 are characterized by a high V_p in the lower portion of the transition zone, approximately 2% faster than that of the iasp91 average Earth model.

models that included a small (1–2% contrast in V_p) discontinuity near a depth of 520 km. Under this category of models, C27 is our best fitting model that matches the seismogram at a distance of 2300 km in detail, particularly regarding the location of cusp B" (Figure 3b). For the other stations along this profile, synthetic seismograms generated from models C34 and C27 match observations equally well (Figure 3). With a small jump in V_p in the middle of the transition zone, model C27 decreases the linear gradient in V_p to $4.86\pm0.2 \times 10^{-3}$ km/s/km in each of the two layers straddled by the 520-km discontinuity. To match the observed waveforms, results of modeling show that the discontinuity can occur over depths up to 10–15 km, but no more than 20 km. Otherwise, models C27 and C34 are quite similar (Figure 4). In particular, in the lower part of the transition zone, V_p in both models are approximately 2% faster than the iasp91 velocity model.

The existence of the 520-km discontinuity as a global feature is controversial [cf. *Shearer*, 1996; *Benz and Vidale*, 1993; *Bock*, 1994; *Cummins et al.*, 1992; *Jones et al.*, 1992]. Although model C27 seems to explain data along profile 11 better than models without a 520-km discontinuity, we have no other evidence to corroborate the existence of such a discontinuity beneath the northern Philippine Sea. Therefore, we shall use the simple model C34 to describe the northern Philippine Sea anomaly. Given the limited aperture of the broadband profile, one may question whether all features of the transition zone associated with model C34 can be confidently resolved. In the next few sections we shall revisit these features as they are borne out by short-period data.

Short-period data. Using short-period data from the CWB-TTSN array in Taiwan, we find that portions of the mantle transition zone sampled by several profiles are close to the area examined by profile 11. In particular, the source-receiver geometry for profile 10 is approximately the reverse of profile 11, minimizing the possible effect of dipping structures (Figure 1). Indeed, similar results from profiles 10 and 11 support the notion that a laterally homogeneous model is sufficient to explain the northern Philippine Sea anomaly. Data and results of our analysis for profile 10 are shown in Figure 5, whose layout of seismograms is similar to that of Figure 3. Details of processing and selection of data for the CWB-TTSN array appear in Appendix B.

In Figure 5, both the relative travel times and amplitudes of later arrivals with respect to the first arrival are well explained by synthetic seismograms generated from model C34. Notice that first, no late arrivals of large amplitude are observed close to the near end of the array (distance of ~1950 km; Figure 5a). The only likely candidates for large, late arrivals near a distance of 2000 km are phases associated with cusp C, at the near end of the triplication due to the 660-km discontinuity (Figure 5c). Thus the short span of branches BC and CD is consistent with a small contrast in V_p across the 660-km discontinuity, characteristic of model C34 but approximately half the contrast predicted by the iasp91 average Earth model (Figures 4 and 5c).

Second, at distances larger than 2000 km the effect of a small contrast in V_p across the bottom of the transition zone is also observed from the arrival times of phases associated with turning refraction (branch CD) and pseudo-reflection (branch BC) in the transition zone. Such arrivals occur within 5 s of the first arrivals (Figure 5a), approximately 2–3 s earlier than predictions based on the iasp91 model (Figure 5c). In model C34 the early arrival times are a direct consequence of fast V_p in the lower transition zone. The alternative interpretation that V_p just below the 660-km discontinuity is anomalously slow is inconsistent with the move-out of observed first arrivals from broadband data along profile 11 (Figure 3).

Finally, judging from the simple pulse shape of the first arrival at the near end of the array, the total duration of the source time function is approximately only 1 s or less (Figure 5a). Thus at distances of 2075–2200 km, large arrivals associated with the cusp B' are interpreted to be among the sequence of pulses that occur within 5 s of the first arrivals (Figure 5a). The assertion that cusp B' terminates beyond a distance of 2200 km is consistent with our identification of this cusp at the very near end of the broadband profile (P11) near 2300 km (Figure 3). The location of this cusp was also correctly predicted by model C34 along profile 5, to be discussed in Figure 11.

For the short-period profiles in general, the average spacing between stations is only 20 km, and the arrival time of each phase can be determined to within ±0.5 s.

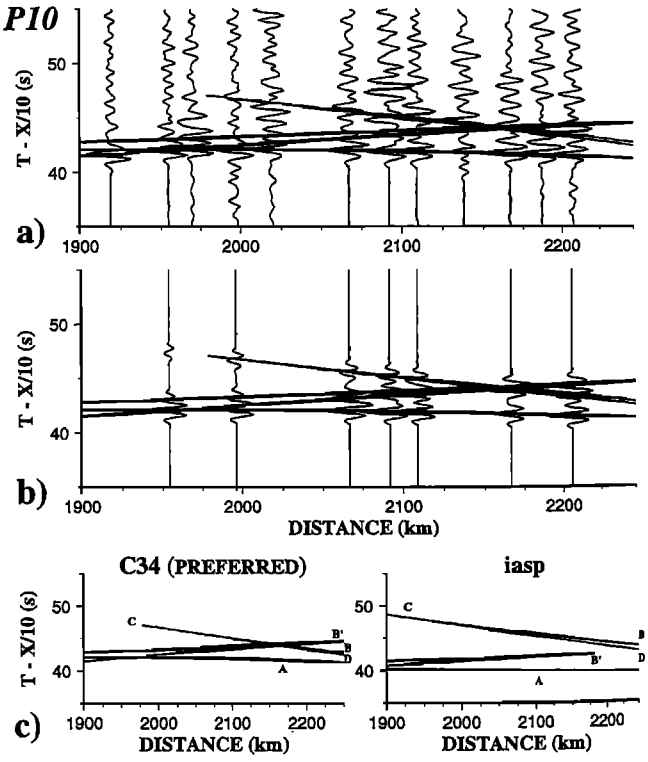

Figure 5. Results for profile 10, approximately sampling the same region as profile 11 but with a reversed source-receiver configuration (Figure 1). (a) Observed seismograms (solid traces) overlain by predicted travel times of the preferred model C34 (smooth curves). (b) Synthetic seismograms (solid traces) and travel times predicted by model C34. Both the timing and amplitude of synthetic waveforms match observations shown in Figure 5a. (c) Comparison of travel time curves predicted by models C34 and iasp91. Notice differences in the locations of cusps C and B' and in the timing of BC–CD branches with respect to first arrivals.

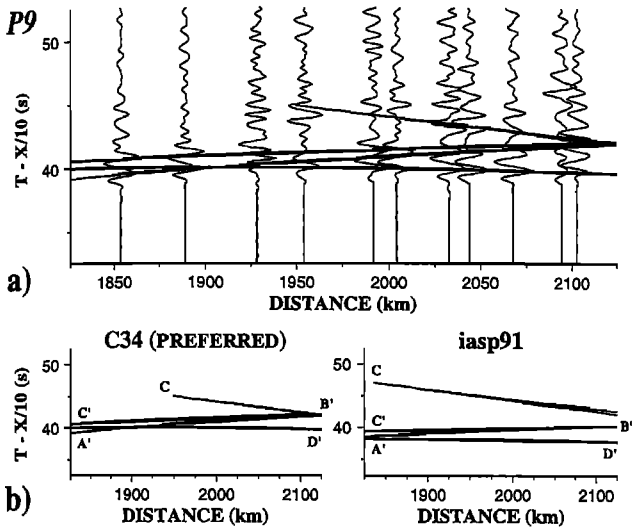

Figure 6. Results for profile 9, sampling a region between profiles 10 and 11 within the northern Philippine Sea anomaly (Figure 1). (a) Observed seismograms (solid traces) overlain by predicted travel times of the preferred model C34 (smooth curves). (b) Comparison of travel time curves predicted by models C34 and iasp91. Notice differences in the location of cusp C and in the timing of late arrivals with respect to first arrivals.

The latter is equivalent to an uncertainty of ±0.7 s for differential travel times. Such a resolution in space and time is comparable to that expected from the uncertainties cited earlier based on modeling of broadband waveforms.

Along profiles 5–9 and profile 12, model C34 also provides a satisfactory explanation for observed seismograms. Figure 6 shows another example, profile 9. The apertures of profiles 9 and 10 are similar, but profile 9 incorporates data from smaller epicentral distances. The termination of cusp C near the distance of 1950 km is particularly clear in this case (Figure 6), corroborating a small contrast in V_p across the 660-km discontinuity in model C34. Along profiles 5–12 the turning points of rays sample a region of approximately 500×500 km^2 within which V_p of the transition zone appears to be laterally uniform (Figure 1). This result corroborates that the northern Philippine Sea anomaly is mainly a subhorizontal feature [*Fukao et al.*, 1992; *van der Hilst et al.*, 1991, 1993].

Lateral Extent of the Anomaly

Southern termination of the anomaly. The anomaly terminates to the southeast and south of the region sampled by profile 12, as no anomalous V_p in the transition zone is detected along profiles 13–16 (Figure 1). For instance, the horizontal separation between regions sampled by profiles 12 and 14 is approximately 300 km, yet observations along profile 14 can be fully accounted for by the iasp91 model and are clearly inconsistent with a fast V_p in the transition zone.

Data plotted in Figure 7a show that in this particular layout, move-outs of all later arrivals have negative slopes over the entire range of profile 14. Time delays between secondary and first arrivals decrease from approximately 4 s at a distance of 2300 km to about 2 s at 2450 km. Such a move-out is precisely that predicted by the iasp91 model for refraction (branch CD) and pseudo-reflections (branch BC) bottoming in the transition zone. Were the lower portion of the transition zone to have anomalously high V_p, such as in model C34, these delays must be considerably smaller than those observed (Figure 7b).

Notice that in Figure 7b, move-outs of arrivals associated with the triplication due to the 400-km discontinuity, if any, will show a positive slope (e.g., branch B'C'; Figure 2). Such arrivals are absent in the data (Figure 7a). The absence of cusp B' in profile 14 indicates that this profile samples the mantle transition zone outside the southern boundary of the northern Philippine Sea anomaly (Figure 1). In contrast, data from profile 12 can be explained by model C34 but are clearly incompatible with model iasp91.

The southern limit of the anomaly is further constrained by profile 13, whose source occurs on the southern edge of the Izu–Bonin arc, and by profiles 15 and 16, whose sources are events along the Mariana arc (Figure 1). Although no cusps are present in the waveforms sampled along profile 13, the observed differences in timing between later and first arrivals are consistent with the iasp91 model (Figure 8). These differences decrease from approximately 3 s at the near end of the array to slightly less than 2 s at the far end. In contrast, model C34 predicts a nearly constant interval of approximately 1 s across the entire array (Figure 8b). Similarly, data from all three profiles (13, 15, and 16) are consistent with the iasp91 model, with no indication of an anomalously fast V_p in the transition zone south or east of profile 12. These observations lead us to conclude that the southeastern edge of the northern Philippine Sea anomaly terminates between the regions sampled by profiles 12 and 13 (Figure 1).

Northern termination of the anomaly. The northwestern limit of the northern Philippine Sea anomaly

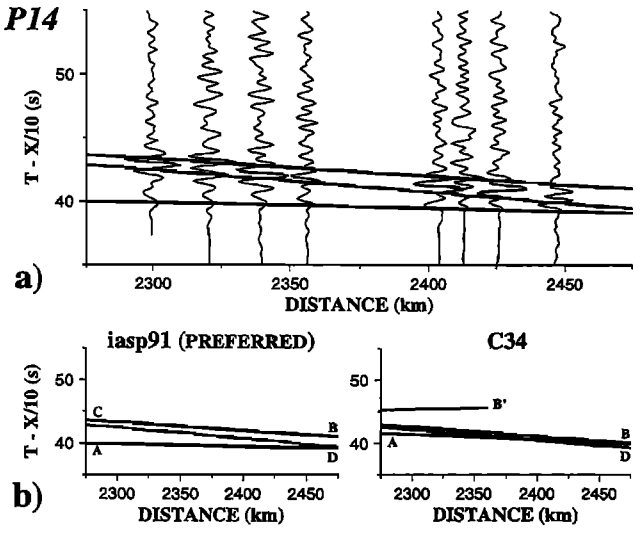

Figure 7. Results for profile 14, sampling the mantle transition zone due east of Taiwan beneath the northern Philippine Sea (Figure 1). (a) Observed seismograms (solid traces) overlain by predicted travel times of the preferred iasp91 model (smooth curves). (b) Comparison of travel time curves predicted by models C34 and iasp91. Notice differences in the locations of cusp B' and in the timing of later arrivals with respect to first arrivals.

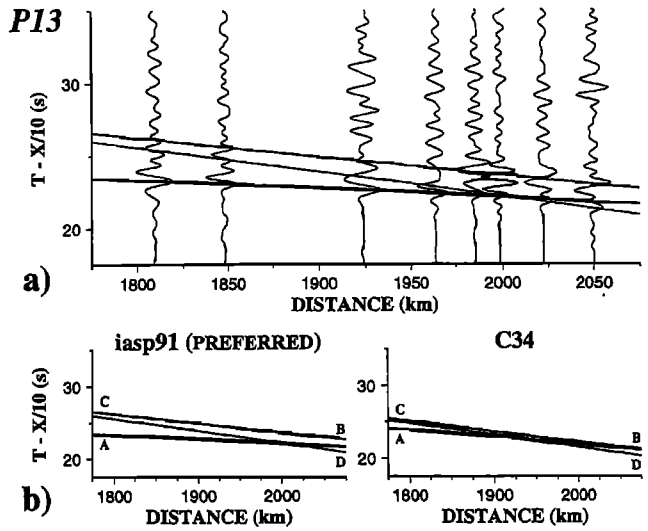

Figure 8. Results for profile 13, sampling a region just to the east of the northern Philippine Sea anomaly (Figure 1). (a) Observed seismograms (solid traces) overlain by predicted travel times of the preferred iasp91 model (smooth curves). (b) Comparison of travel time curves predicted by models C34 and iasp91. When compared with the observations, time intervals between later and first arrivals predicted by model C34 are too small and nearly constant across the array.

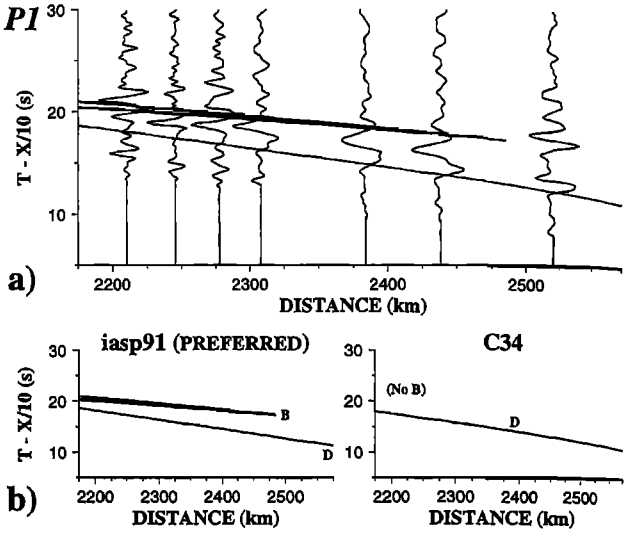

Figure 9. Results for profile 1, sampling the transition zone in the back arc region beneath South Korea (Figure 1). (a) Observed seismograms (solid traces) overlain by predicted travel times of the preferred iasp91 model (smooth curves). On the basis of detailed investigation of the source-time function [*Chen et al.*, 1996] we used the arrival times of the second, larger pulse of observed signals. (b) Comparison of travel time curves predicted by models C34 and iasp91. No triplication is predicted by model C34 at distances greater than 2175 km.

is largely constrained by profiles 1, 2, and 5 (Figures 1 and 9–11). The source for profile 1 is a recent, large earthquake whose source time function consists of two bursts of seismic moment release. *Chen et al.* [1996] studied this event in detail and reported that each of the two body wave pulses has a duration of approximately 4 s, with a time separation of approximately 4 s between them. Consequently, we have picked the first arrivals according to the onset of the second, larger burst of moment release in Figure 9a.

Since the source depth is well below the 400-km discontinuity (Table 1), only the triplication due to the 660-km discontinuity can be expected from this profile (Figure 2). A prominent second arrival is clearly observed over the entire distance range of this profile (Figure 9a). Delay times and move-out of this second phase in relation to the first arrivals are well explained by the iasp91 model, placing cusp B at a distance of approximately 2500 km (Figure 9a). Incidentally, like profile 10 (Figure 5), short-period waveforms from this event can be matched by synthetic waveforms. These observations cannot be explained by a high V_p in the transition zone, because such an anomaly would reduce the contrast in V_p across the 660-km discontinuity and place cusp B at a distance of several hundred kilometers smaller than that observed (Figure 9b). This particular result is consistent with that of *Tajima and Grand* [1995], who studied a similar problem beneath the Japan Sea.

In fact, profile 2 provides evidence that the anomaly does not extend beyond the west coast of southern Japan (Figure 1). At the near end of the array (~1900 km), arrivals from branches BC and CD are delayed by more than 4 s from the first arrivals (Figure 10a). These arrival times agree well with predictions of the iasp91 model but are clearly incompatible with those of model C34, which predicts a delay of only 1.5 s at this distance (Figure 10b).

In contrast, profile 5 indicates that the northern Philippine Sea anomaly does extend beneath the southernmost tip of Japan near a latitude of 30°N (Figure 1). At distances near 1800 km, arrivals from

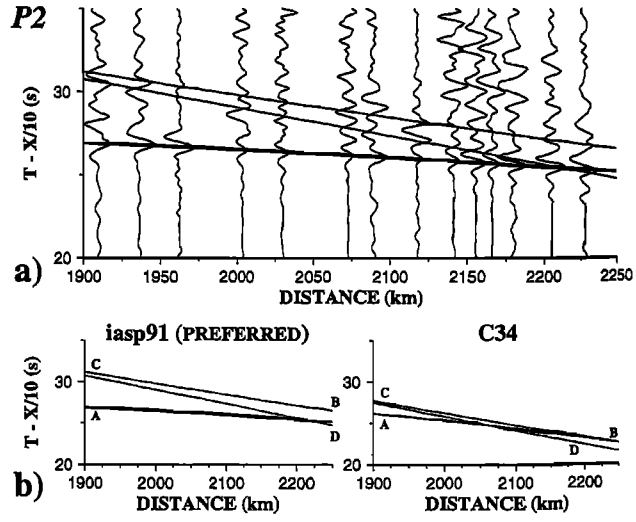

Figure 10. Results for profile 2, sampling the mantle transition zone in the back arc region just west of Kyushu (Figure 1). (a) Observed seismograms (solid traces) overlain by predicted travel times of the iasp91 model (preferred, smooth curves). (b) Comparison of travel time curves predicted by models C34 and iasp91. The difference in predicted move-outs of later arrivals is most conspicuous at the near end of the array (1900 km).

branches BC and CD are observed within 4 s of the first arrival, as predicted by model C34 (Figure 11a). Meanwhile, model iasp91 predicts too large a delay of more than 6 s at the same distance (Figure 11b). Moreover, arrivals from cusp B' predicted by model C34 are also present in the data near the distance of 1775 km (Figure 11a).

Thus the termination of the northern Philippine Sea anomaly must have occurred within the 300 km distance between the regions sampled by profiles 2 and 5 (Figure 1). However, the exact northern limit of the anomaly cannot be further refined. Along profiles 3 and 4, predicted differences in arrival times and move-outs between models C34 and iasp91 are small. Consequently, we cannot confidently resolve whether regions sampled by profiles 3 and 4 are part of the northern Philippine Sea anomaly or a transitional region near the edge of the anomaly.

In summary, results of 16 seismic profiles indicate that the lateral extent of the anomaly seems much smaller than that inferred from travel time tomography of first arrivals [cf. *Fukao et al.*, 1992; *van der Hilst et al.*, 1991, 1993]. The most pronounced anomaly in the transition zone is mapped out by profiles 5–12, approximately centered just east of the Ryukyu arc beneath the northwestern corner of the Philippine Sea (Figure 1). Within this region the anomaly can be approximated as a subhorizontal, laterally uniform feature in the transition zone. However, instead of centering near a depth of approximately 530±40 km [*Fukao et al.*, 1992; *van der Hilst et al.* , 1991, 1993], fast V_p appears to occur in the lower portion of the transition zone, reducing the contrast of V_p across the 660-km discontinuity from approximately 6% to 3% (Figure 4).

Interpretation and Discussion

Our results bolster the interpretation that the northern Philippine Sea anomaly is caused by remnants of subducted Pacific lithosphere, even though we disagree with the assertion of *Fukao et al.* [1992] and *van der Hilst et al.* [1991, 1993] that the anomaly mainly occurs in the middle of the transition zone. The reason is twofold. First, since the thermal constant for old oceanic lithosphere is approximately 80 Ma [e.g., *Parsons and Sclater*, 1977], cold Pacific lithosphere should remain negatively buoyant for tens of millions of years after subduction.

Second, since the phase transition across the 660-km discontinuity has a negative Clapeyron slope [e.g., *Ito and Takahashi*, 1989], this discontinuity presents a resistance to slab penetration [*Turcotte and Schubert*, 1971]. As subduction continues along the Izu–Bonin [*van der Hilst and Seno*, 1993], negative buoyancy would rest the slab just above the 660-km discontinuity where considerable resistance to slab penetration is expected [*Turcotte and Schubert*, 1971]. The presence of a cold slab should increase the depth to the 660-km discontinuity. *Shearer* [1991] reported that on average, the difference in depths to this discontinuity between large-scale tectonic provinces is of the order of 10 km. However, we cannot prove that such a depression of the 660-km discontinuity exists under the northern Philippine Sea anomaly, because this value is approximately the limit of resolution in our data for this particular parameter.

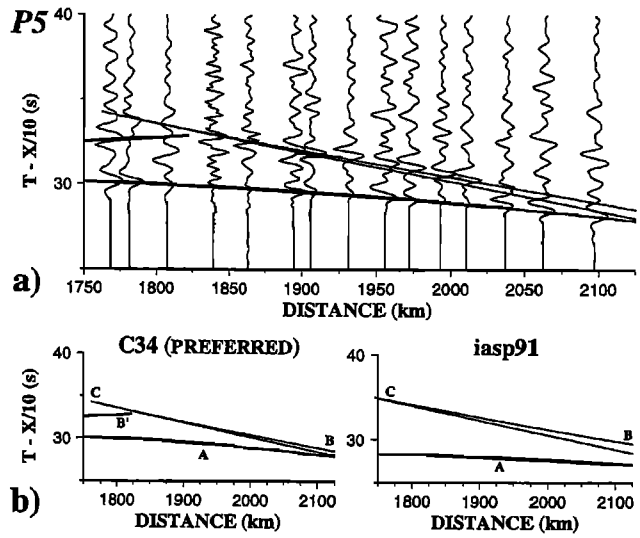

Figure 11. Results for profile 5 near the northernmost limit of the northern Philippine Sea anomaly (Figure 1). (a) Observed seismograms (solid traces) overlain by predicted travel times of model C34 (smooth curves). (b) Comparison of travel time curves predicted by models C34 and iasp91. Note that the presence of cusp B' is predicted correctly by model C34.

If the northern Philippine Sea anomaly is due to subducted lithosphere of the Pacific plate, an obvious interpretation is that the high V_p is a result of cold temperatures associated with subducted lithosphere. We estimated the temperature difference, ΔT_{max}, between the coldest interior of the slab and the surrounding asthenosphere by an analytical approximation of *McKenzie* [1970]. Since we are interested only in the temperature difference between the asthenosphere and subducted slab, adiabatic heating and latent heat associated with phase transformation have no effect on ΔT_{max}. We specified a slab length of 1500 km, slab thickness of 100 km [*van der Hilst and Seno*, 1993], and convergence rate of 45 mm/yr [*Seno et al.*, 1993] in our calculations. Values for the other parameters are assumed to be the same as those of *Molnar et al.* [1979]. The estimated ΔT_{max} is 300°K. Thus, on average, the suspected slab remnant is approximately 150°K cooler (ΔT) than the asthenosphere.

It is important to bear in mind that even at relatively shallow depths, all estimates of ΔT are subject to considerable uncertainty [e.g., *Peacock*, 1996]. Using parameters whose values are similar to those listed above, we compared the results from different schemes of thermal modeling. For instance, for a 60°-dipping slab at a depth of 400 km where a number of published results are available, the analytical solution seems to underpredict the ΔT. The amount of underprediction, however, ranges from as small as 20% up to nearly 60%, when compared with the finite element model of *Davies and Stevenson* [1992] and a finite difference model of *Stein and Stein* [1996], respectively. Thus our estimated ΔT for the northern Philippine Sea anomaly is likely to be uncertain by at least the same magnitude.

Using a temperature derivative of -0.4 to -0.5 m/s °K [e.g., *Kern*, 1982; *Creager and Jordan*, 1986], we expect a ΔT of 150°K to raise the V_p by 0.06–0.075 km/s when

averaged over the thickness of the slab. If the temperature anomaly is 60% larger, as suggested by the models of *Stein and Stein* [1996], V_p will increase by 0.10–0.12 km/s. In this case, thermal effect alone may be sufficient to explain the anomaly in V_p observed at a depth near 580 km under the northern Philippine Sea. On the other hand, if the ΔT is only 20% greater, as is suggested by the calculations of *Davies and Stevenson* [1992], petrological effects may be needed to explain the observed anomaly in V_p, unless the actual value of V_p is at the lowest possible bound allowed by uncertainties in our measurements. It is interesting to note that a ΔT in excess of 200°K is expected to depress the depth of the 660-km discontinuity by approximately 20 km [*Ito and Takahashi*, 1989; *Shearer*, 1991], an effect we did not observe.

Minerals expected to be stable under temperature and pressure conditions in the transition zone fall into three categories [*Duffy and Anderson*, 1989]. First is β- and γ-spinel, both being high-pressure forms of olivine with fast V_p. Second is a garnet-majorite solid solution, characterized by V_p values slower than those of spinels. Third is a minor component, jadeite, a clinopyroxene with very slow V_p. If the temperature effect associated with a cold subducted slab is much less than 250°K, the high value of observed V_p associated with the northern Philippine Sea anomaly suggests that β- and γ-spinel are the only candidates that can account for an additional increase in V_p. If so, the lower portion of the transition zone under investigation must be enriched in high-pressure forms of olivine relative to the average Earth.

In general terms this petrologic interpretation is consistent with the notion that this anomaly is a result of subducted Pacific lithosphere, trapped just above the 660-km discontinuity. First, both travel time tomography and our results indicate that the anomaly is a subhorizontal feature, probably extending continuously westward from the tip of the Izu–Bonin Wadati-Benioff zone [*Fukao et al.*, 1992; *van der Hilst et al.*, 1991, 1993]. This geometry suggests that original layering of subducted Pacific lithosphere would be largely intact. The bulk of subducted lithosphere is expected to be depleted mantle material (i.e., relatively enriched in olivine), overlain by a veneer of enriched eclogite crust. A remnant of thick, depleted lithospheric mantle is a suitable candidate for fast V_p in the bottom portion of the transition zone.

Second, *O'Neill et al.* [1993] reported that hydrous, calcium-rich garnet, likely to be stable under high pressures, has an extremely low seismic wave speed. Thus a veneer of hydrothermally altered oceanic crust, which is expected to turn into eclogite (mainly garnet and clinopyroxene) if it is subducted with the rest of the lithosphere, may be sufficient to account for the relatively slow V_p in the upper portion of the transition zone beneath the northern Philippine Sea. This interpretation is speculative, and the relatively slow V_p over a large thickness in the upper portion of the transition zone is difficult to explain.

Conclusions

Using 16 seismic profiles, each including relevant arrivals from triplications of travel time curves associated with the mantle transition zone, we constrained three-dimensional variations in V_p associated with the northern Philippine Sea anomaly. Azimuthal coverage of the profiles indicate that the lateral extent of the anomaly is much smaller than that inferred from travel time tomography using mainly first arrivals. Nonetheless, the anomaly does stand out as a subhorizontal, laterally uniform feature in the transition zone beneath the northwestern corner of the Philippine Sea (Figure 1).

On the basis of seismic rays whose turning points occur within the anomaly, an important characteristic of the anomaly is that fast V_p occurs in the lower portion of the transition zone, reducing the contrast in V_p across the 660-km discontinuity to approximately 3% (Figure 4). Although these features differ from images of travel time tomography, constraints presented here actually help bolster the interpretation that the northern Philippine Sea anomaly is associated with subducted Pacific lithosphere. On the basis of estimates of temperature fields associated with subduction, V_p of stable mineral assemblages under mantle conditions, and expected layering within subducted slabs, we interpret that a remnant of subducted Pacific lithosphere is trapped in the transition zone just above the 660-km discontinuity.

Appendix A: Processing of Pre-POSEIDON Broadband Data

Station Corrections

The Pre-POSEIDON stations are located in Japan near the junction of the Pacific, Philippine Sea, and Honshu plates where the geology is complex [e.g., *DeMets*, 1992]. On the basis of short-period *P* arrivals, station corrections (statics) of the order of ±1 s have been reported for this general area [e.g., *Hager and Clayton*, 1989]. Azimuth-dependent station corrections of similar magnitude have also been reported across the Gräfenberg broadband array in Germany [*Weber*, 1994]. We determined statics for the Pre-POSEIDON stations by taking weighed averages of travel time residuals from earthquakes at teleseismic distances (Table A1).

Within the 1-year period of May 1993 to May 1994 we were able to determine precise arrival times from eight large teleseismic earthquakes whose epicentral distances varied from 30° to 90°. In this distance range, complications due to triplications in the upper mantle and phases interacting with the core are minimized. For each

Table A1. Hypocenter Information of Calibration Earthquakes

Date	Origin Time, UT	Latitude, °N	Longitude, °E	Depth, km	m_b
May 11, 1993	1826:51.3	7.22	126.57	59	6.1
May 15, 1993	0155:38.8	7.23	126.64	31	5.6
Aug. 4, 1993	1131:18.0	-1.63	99.62	32	5.9
Aug. 29, 1993	0957:54.9	-7.01	129.56	147	5.8
Sept. 1, 1993	1148:38.4	-4.33	102.57	71	5.8
Sept. 29, 1993	1116:03.5	0.49	121.53	97	6.1
Dec. 9, 1993	0432:19.5	0.49	126.00	15	6.5
Dec. 9, 1993	1138:27.9	0.43	125.89	16	6.3

Values of parameters are from the monthly listing of *Preliminary Determination of Epicenters* (PDE).

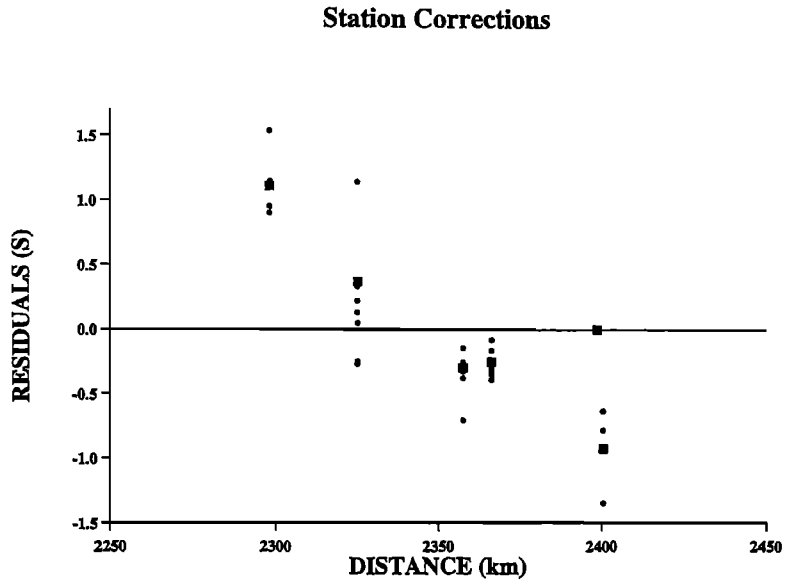

Figure A1. Travel time residuals at five Pre-POSEIDON stations (solid circles) used in Figure 3 relative to global station MAJO, whose absolute residual is close to zero. At each station the solid square shows the station correction that is a weighed average of residuals. The events (Table A1) are chosen with back azimuths appropriate for the geometry of profile 11. Travel times predicted by iasp91 are used as the reference model.

earthquake the back azimuths are within a ±20° range from the source-receiver geometry of profile 11. We then calculated travel time residuals, using the hypocenter information of the Monthly Listing of the Preliminary Determination of Epicenters and the iasp91 travel time curves [*Kennett and Engdahl*, 1991].

Assuming Gaussian statistics and taking into account uncertainties in reading arrival times, we calculated the correction for each station as weighted averages of travel time residuals with respect to station MAJO, a long-standing, standardized global seismograph station whose arrival times have often been included in building reference Earth models (Figure A1). The resulting station corrections are approximately ±1 s, consistent with values reported by *Weber* [1994] and *Hager and Clayton* [1989]. Note that if station corrections were not applied, the move-out of first arrivals shown in Figure 3 would have exceeded 13.5 km/s (in a spherical Earth), an unrealistically fast V_p for the transition zone or the lower mantle.

Finally, to match the absolute arrival time of cusp B' shown in Figure 3, the thin (1.4 km) veneer of sediments in the model of *Erdogan and Nowack* [1993] is replaced by extending their upper crustal layer to the surface.

Source Parameters of the Event on May 18, 1993

Using the *P* wave train from the near real time data retrieval system SPYDER of the Data Management Center of the Incorporated Research Institutions for Seismology (IRIS DMC), we determined the focal mechanism, the depth, the scalar seismic moment, the duration, and the shape of the far-field source time function of this event by waveform inversion. This technique analyzes *P* and *SH* wave trains by minimizing the differences between observed and synthetic seismograms in a least squares sense. This algorithm was originally developed by *Nábelek* [1984] to investigate shallow earthquakes. *Glennon and Chen* [1993, 1995b] and *Chen* [1995] modified Nábelek's routines to study deep earthquakes, and we have used the same procedure here. The readers are referred to those papers for technical details.

Figure A2 shows the result of the inversion. The source depth of this event is determined to be approximately 169±5 km. This is a necessary step in our analysis because to first order, erroneous source depth maps into erroneous epicentral distances across the entire array. Inspection of direct *P* phases at teleseismic distances indicated that the main burst of moment release was preceded by a small precursor (Figure A2). Consequently, we enhanced the high-frequency component of the signals recorded at Pre-POSEIDON stations by using the teleseismic, direct *P* phase recorded at COL as the basis for deconvolution. The signal at COL was chosen because this station lies in the same general azimuth of the source-receiver configuration for profile 11. Any effect of directivity for this station is approximately the same as the effects at Pre-POSEIDON stations.

In fact, strong directivity in the general direction of south is evident from the narrow pulse width at CTAO (Figure A2). The source model used in Figure A2 is a Haskell line source with a rupture velocity of 4 km/s toward south-southwest. Consequently, only the direct *P* pulse recorded at COL has the appropriate azimuth to be used as a basis for deconvolving the Pre-POSEIDON data along profile 11.

In terms of tectonics this earthquake is unusual. The Wadati-Benioff zone of the source region is associated with the east dipping slab of the South China Sea under the Luzon arc [e.g., *Hamburger et al.*, 1983]. The focal mechanism of the earthquake, strike 203°, dip 44°, and rake -150°, has an east-northeasterly plunging *P* axis

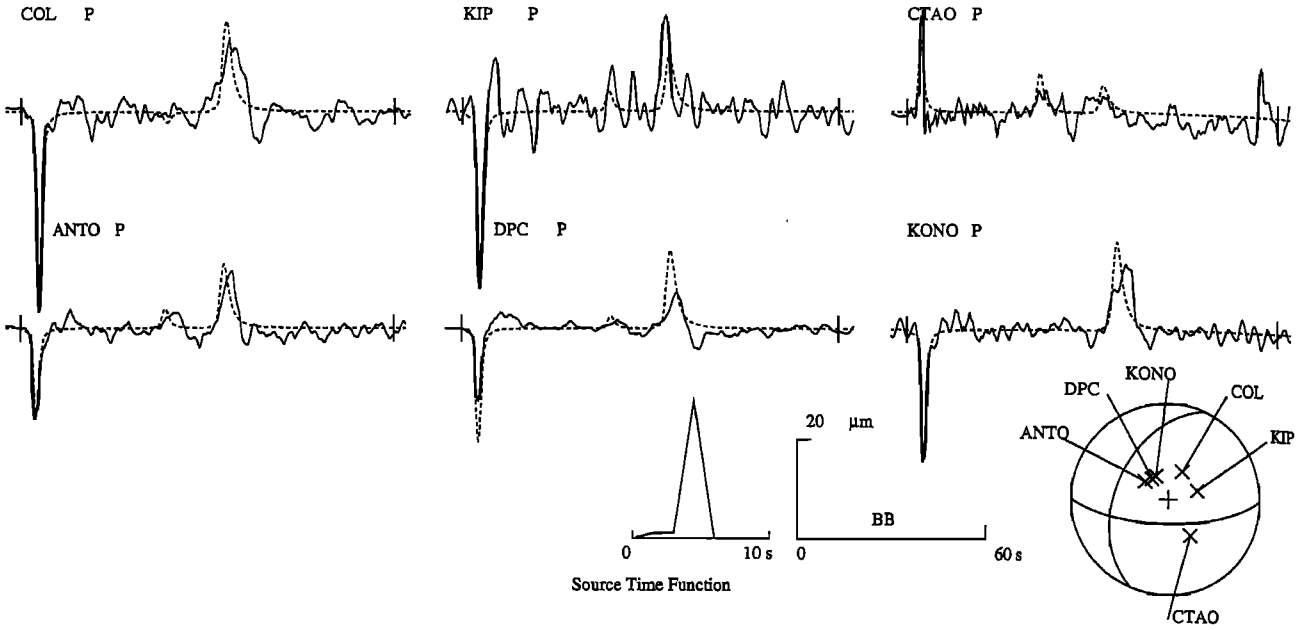

Figure A2. Comparison between observed (solid traces) and synthetic broadband *P* wave trains (dashed traces) at selected teleseismic stations. After normalization to an epicentral distance of 50°, amplitudes of both observed and synthetic ground displacements are plotted with a common absolute scale. Orientations of nodal surfaces for direct *P* phases and locations of observations on the focal sphere are shown in equal-area projection of the lower hemisphere of the focal sphere. Vertical bars on seismograms indicate time windows used in the inversion. The shape of the source-time function is also plotted. Notice the narrow pulse width at CTAO, indicating strong directivity toward the general direction of south.

(Figure A2), indicating downdip compression in the subducting lithosphere. Such a pattern of strain is rare at intermediate depths [e.g., *Kao and Chen*, 1991].

Appendix B: Processing of CWB-TTSN Short-Period Data

The present configuration of the combined CWB-TTSN array includes 75 three-component, short-period stations densely located over an aperture of approximately 3.5° × 1.5°. The array has been operated jointly by the Central Weather Bureau and the Institute of Earth Sciences, Academia Sinica. The TTSN network began digital recording in July 1987, with only vertical component seismographs sampled at 100 Hz [*Wang*, 1989]. In March 1991 the CWB network began recording three-component data at the same sampling rate. For both networks, data are archived for a 3 min duration when triggered by an event. Since the main purpose of the CWB-TTSN array is to record local and regional earthquakes, data for few teleseismic events are retained.

We searched all available data and selected seismograms that satisfy the following criteria: (1) on-scale recordings with high S/N ratios; (2) signals produced by intermediate- and deep-focus earthquakes to avoid potential interference from *pP* and *sP* or any effects of structural complexity above the source; (3) epicentral distances within 20°±5° where turning points of rays associated with triplications of travel time curves are expected to mainly sample the transition zone of the mantle; and (4) back azimuths appropriate for the target area.

The selected data are down-sampled to 25 Hz after anti-alias filtering. For display and modeling purposes we then applied a zero-phase (acausal), sixth-order Butterworth filter, with bandpass corner frequencies set at 1.0 and 0.1 Hz. Without reliable estimates of station corrections, average time shifts between observed and synthetic first arrivals are typically near 3 s, with occasional values as small as 1 s to as large as 5 s. In nearly all cases there is redundancy in data coverage when seismic profiles are plotted. To avoid clutter, we showed only a small number of traces that more or less uniformly cover the entire aperture of each profile in Figures 5–9. In addition, stations located in sedimentary basins were not used, as long coda of the first arrival often obscured later arrivals on the same seismogram.

Acknowledgments. Chu-Yung Chen and J. D. Bass guided us through mantle petrology, and we benefited from discussion with S. Grand, B.-Y. Kuo, T. Lay, and J. Vidale. In particular, S. Grand offered many specific advises, and S. Stein lent help in the modeling of thermal structures. W.-J. Su, Y. J. Chen, and an anonymous reviewer offered helpful suggestions. We are grateful to H. Kawakatsu for answering many questions regarding Pre-POSEIDON data. We also thank K. Shimazaki, T. C. Shin, and Y. H. Yeh for permitting us access to Pre-POSEIDON and CWB-TTSN data. Teleseismic data were collected from the IRIS DMC. This research was supported by NSF grants EAR94-04809 and EAR93-16012 (W.-P.C.) and grant EAR94-05167 (R.L.N.).

References

Anderson, D. L., *Theory of the Earth*, 366 pp., Blackwell Sci., Cambridge, Mass., 1989.

Benz, H. M., and J. E. Vidale, Sharpness of upper mantle discontinuities determined from high-frequency reflections, *Nature*, *365*, 147–150, 1993.

Bock, G., Synthetic seismogram images of upper mantle structure: No evidence for a 520-km discontinuity, *J. Geophys. Res.*, *99*, 15,843–15,851, 1994.

Chapman, C. H., A new method for computing synthetic seismograms, *Geophys. J. R. Astron. Soc.*, *54*, 481–518, 1978.

Chapman, C. H., J.-Y. Chu, and D. G. Lyness, The WKBJ seismogram algorithm, in *Seismological Algorithms: Computational Methods and Computer Programs*, edited by D. J. Doornbos, pp. 47–74, Academic, San Diego, Calif., 1988.

Chen, W.-P., *En echelon* ruptures during the great Bolivian earthquake of 1994, *Geophys. Res. Lett.*, *22*, 2261–2264, 1995.

Chen, W.-P., L.-R. Wu, and M. A. Glennon, Characteristics of multiple ruptures during large deep-focus earthquakes, in *Subduction Top to Bottom*, *Geophys. Monogr. Ser.*, vol. 96, edited by G. E. Bebout et al., pp. 357–368, AGU, Washington, D. C., 1996.

Creager, K. C., and T. H. Jordan, Slab penetration into the lower mantle, *J. Geophys. Res.*, *89*, 3031–3049, 1984.

Creager, K. C., and T. H. Jordan, Slab penetration into the lower mantle beneath the Mariana and other island arcs of the Northwest Pacific, *J. Geophys. Res.*, *91*, 3573–3589, 1986.

Cummins, P. R., B. L. N. Kennett, J. R. Bowman, and M. G. Bostock, The 520-km discontinuity?, *Bull. Seismol. Soc. Am.*, *82*, 323–336, 1992.

Davies, J. H., and D. J. Stevenson, Physical model of source region of subduction zone volcanics, *J. Geophys. Res.*, *97*, 2037–2070, 1992.

DeMets, C., A test of present-day plate geometries for northeast Asia and Japan, *J. Geophys. Res.*, *97*, 17,627–17,635, 1992.

Ding, X. Y., and S. P. Grand, Seismic structure of the deep Kurile subduction zone, *J. Geophys. Res.*, *99*, 23,767–23,786, 1994.

Duffy, T. S., and D. L. Anderson, Seismic velocities in mantle minerals and the mineralogy of the upper mantle, *J. Geophys. Res.*, *94*, 1895–1912, 1989.

Erdogan, N., and R. L. Nowack, Slant-stack velocity analysis for one-dimensional upper mantle structure using short-period data from MAJO, *Pure Appl. Geophys.*, *141*, 1–24, 1993.

Fukao, Y., M. Obayashi, H. Inoue, and M. Nenbai, Subducting slabs stagnant in the mantle transition zone, *J. Geophys. Res.*, *97*, 4809–4822, 1992.

Glennon, M. A., and W.-P. Chen, Systematics of deep-focus earthquakes along the Kuril-Kamchatka Arc and their implications on mantle dynamics, *J. Geophys. Res.*, *98*, 735–769, 1993.

Glennon, M. A., and W.-P. Chen, Travel times from earthquakes near southern Kuril and their implications on the fate of subducted lithosphere, *Phys. Earth Planet. Interior.*, *88*, 177–191, 1995a.

Glennon, M. A., and W.-P. Chen, Ruptures of deep-focus earthquakes in the northwestern Pacific and their implications on seismogenesis, *Geophys. J. Int.*, *120*, 706–720, 1995b.

Hager, B. H., and R. W. Clayton, Constraints on the structure of mantle convection using seismic observations, flow models, and the geoid, in *Mantle Convection: Plate Tectonics and Global Dynamics, The Fluid Mechanics of Astrophysics and Geophysics*, vol. 4, edited by W. R. Peltier, pp. 657–763, Gordon and Breach, Newark, N. J., 1989.

Hamburger, M. W., R. K. Cardwell, and B. L. Isacks, Seismotectonics of the northern Philippine island arc, in *The Tectonic and Geologic Evolution of Southeast Asian Seas and Islands: Part II*, *Geophys. Monogr. Ser.*, vol. 27, edited by D. E. Hayes, pp. 1–22, AGU, Washington, D. C., 1983.

Ito, E., and E. Takahashi, Postspinel transformations in the system Mg_2SiO_4-Fe_2SiO_4 and some geophysical implications, *J. Geophys. Res.*, *94*, 10,637–10,646, 1989.

Jones, L. E., J. Mori, and D. V. Helmberger, Short-period constraints on the proposed transition zone discontinuity, *J. Geophys. Res.*, *97*, 8765–8774, 1992.

Jordan, T.H., Lithospheric slab penetration into the lower mantle beneath the Sea of Okhotsk, *J. Geophys.*, 43, 473-496, 1977.

Kao, H., and W.-P. Chen, Earthquakes along the Ryukyu–Kyushu arc: Strain segmentation, lateral compression, and the thermomechanical state of the plate interface, *J. Geophys. Res.*, *96*, 21,443–21,485, 1991.

Kennett, B. L. N., Seismic structure and heterogeneity in the upper mantle, in *Relating Geophysical Structures and Processes: The Jeffreys Volume*, *Geophys. Monogr. Ser.*, vol. 76, edited by K. Aki and R. Dmnowska, pp. 53–66, AGU, Washington D. C., 1993.

Kennett, B. L. N., and E. R. Engdahl, Traveltimes for global earthquake location and phase identification, *Geophys. J. Int.*, *105*, 429–465, 1991.

Kern, S., *P*- and *S*-wave velocities in crustal and mantle rocks under the simultaneous action of high confining pressure and high temperature and the effect of the rock microstructure, in *High-Pressure Researches in Geoscience*, edited by W. Schreyer, pp. 15–45, Schweizerbart, Stuttgart, Germany, 1982.

Lay, T., The fate of descending slabs, *Annu. Rev. Earth Planet. Sci.*, *22*, 33–61, 1994.

McKenzie, D. P., Temperature and potential temperature beneath island arcs, *Tectonophysics*, *10*, 357–366, 1970.

Molnar, P., D. Freedman, and J. S. F. Shih, Lengths of intermediate and deep seismic zones and temperatures in downgoing slabs of lithosphere, *Geophys. J. R. Astron. Soc.*, *56*, 41–54, 1979.

Nábelek, J. L., Determination of earthquake source parameters from inversion of body waves, Ph.D. thesis, 361 pp., Mass. Inst. of Technol., Cambridge, 1984.

O'Neill, B., J. D. Bass, and G. R. Rossman, Elastic properties of hydrogrossular garnet and implications for water in the upper mantle, *J. Geophys. Res.*, *98*, 20,031–20,037, 1993.

Parsons, B., and J. G. Sclater, An analysis of the variation of ocean floor bathymetry and heat flow with age, *J. Geophys. Res.*, *82*, 803–827, 1977.

Peacock, S. M., Thermal and petrologic structure of subduction zones, in *Subduction Top to Bottom*, *Geophys. Monogr. Ser.*, vol. 96, edited by G. E. Bebout et al., pp. 357–368, AGU, Washington, D. C., 1996.

Revenaugh, J., and T. H. Jordan, Mantle layering from *ScS* reverberation, 2, The transition zone, *J. Geophys. Res.*, *96*, 19,763–19,780, 1991.

Seno, T., S. Stein, and A. E. Gripp, A model for the motion of the Philippine Sea Plate consistent with NUVEL-1 and geological data, *J. Geophys. Res.*, *98*, 17,941–17,948, 1993.

Shearer, P. M., Seismic imaging of upper-mantle structure with new evidence for a 520 discontinuity, *Nature*, *344*, 121–126, 1990.

Shearer, P. M., Constraints on upper mantle discontinuities from observations of long-period reflected and converted phases, *J. Geophys. Res.*, *96*, 18,147–18,182, 1991.

Shearer, P. M., Transition zone velocity gradients and the 520-km discontinuity, *J. Geophys. Res.*, *101*, 3053–3066, 1996.

Shearer, P. M., and T. G. Masters, Global mapping of topography on the 660-km discontinuity, *Nature*, *355*, 791–796, 1992.

Silver, P. G., R. W. Carlson, and P. Olson, Deep slabs, geochemical heterogeneity and the large-scale structure of mantle convection, *Annu. Rev. Earth Planet. Sci.*, *16*, 477–541, 1988.

Stein, S., and C. A. Stein, Thermo-mechanical evolution of oceanic lithosphere: Implications for the subduction processes and deep earthquakes, in *Subduction Top to Bottom*, *Geophys. Monogr. Ser.*, vol. 96, edited by G. E. Bebout et al., pp. 357–368, AGU, Washington, D. C., 1996.

Tajima, F., and S. P. Grand, Evidence of high velocity anomalies in the transition zone associated with southern Kurile subduction zone, *Geophys. Res. Lett.*, *22*, 3139–3142, 1995.

Turcotte, D. L., and G. Schubert, Structure of the olivine-spinel phase boundary in the descending lithosphere, *J. Geophys. Res.*, *76*, 7980–7987, 1971.

van der Hilst, R. D., and T. Seno, Effects of relative plate motion on the deep structure and penetration depth of slabs below the Izu–Bonin and Mariana island arcs, *Earth Planet. Sci. Lett.*, *120*, 395–407, 1993.

van der Hilst, R. D., E. R. Engdahl, W. Spakman, and G. Nolet, Tomographic imaging of subducted lithosphere below northwest Pacific island arcs, *Nature*, *353*, 37–43, 1991.

van der Hilst, R. D., E. R. Engdahl, and W. Spakman, Tomographic inversion of *P* and *pP* data for aspherical mantle structure below the northwest Pacific region, *Geophys. J. Int.*, *115*, 264–302, 1993.

Wang, J. H., The Taiwan Telemetered Seismographic Network, *Phys. Earth Planet. Inter.*, *58*, 9–18, 1989.

Weber, M., Traveltime and amplitude anomalies at the seismic broadband array GRF, *Geophys. J. Int.*, *118*, 57–74, 1994.

M. R. Brudzinski and W.-P. Chen, Department of Geology, University of Illinois, 245 Natural History Building, 1301 W. Green Street, Urbana, IL 61801. (email: brudzins@uiuc.edu)

B.-S. Huang, Institute of Earth Sciences, Academia Sinica, Taipei, Taiwan.

R. L. Nowack, Department of Earth and Atmospheric Sciences, Purdue University, West Lafayette, IN 47907.

(Received June 19, 1996; revised November 22, 1996;
accepted January 21, 1997.)